Investigations into Sulfobetaine-Stabilized Cu Nanoparticle Formation: Toward Development of a Microfluidic Synthesis

Yujun Song,[†] E. E. Doomes,[†] John Prindle,[‡] Roland Tittsworth,[†] Josef Hormes,[†] and Challa S. S. R Kumar*,[†]

Center for Advanced Microstructures and Devices, Louisiana State University, 6980 Jefferson Highway, Baton Rouge, Louisiana 70806, and Chemical and Biomolecular Engineering Department, 300 Lindy Boggs, Tulane University, New Orleans, Louisiana 70118

Received: November 15, 2004; In Final Form: March 15, 2005

The mechanistic aspects of the formation of sulfobetaine-stabilized copper nanoparticles were investigated by using in situ XANES (X-ray absorption near edge structure), UV−vis spectroscopy, and reaction calorimetry. The tetracoordinated sulfobetaine−Cu(II) complex was reduced to a stable sulfobetaine−Cu(I) complex prior to the formation of sulfobetaine-stabilized copper nanoparticles. The stability of the Cu(I) complex was found to be sensitive to the concentration of the sulfobetaine stabilizer and the addition rate of the reducing agent. It appears to exist primarily as a linear complex. A tetracoordinated Cu(I) complex as an intermediate has also been postulated. Based on the understanding from these investigations, a microfluidic process for copper nanoparticle synthesis was designed by using sulfobetaine−Cu(I) complex as the starting material. When compared with the copper nanoparticles synthesized by a conventional batch process, the microfluidic reactor process provided particles with a smaller size and narrower size distribution. The copper nanoparticles from the microreactor process could also be more easily purified and the particles were relatively stable in air. Both XRD and SAED indicated that the Cu nanoparticles synthesized have fcc structure.

Introduction

Owing to their unique catalytic, electronic, magnetic, and optical properties different from their bulk species, nanoparticles continue to attract the attention of researchers.[1] Synthesis of monodispersed nanoparticles is challenging and especially size and structure controlled syntheses with various techniques are being explored.[2] The optical, electronic, and thermal properties of Cu, Ag, and Au nanoparticles endow them with potential application in electrical and third-order nonlinear optical devices,[3−8] solid dielectric materials,[9] nano-bio materials,[10] and high thermal conductivity nanofluids.[11] Due to their absorption characteristics in the ultraviolet and visible spectral region, these noble metal nanoparticles are also good models to investigate mechanistic aspects of the nanoparticle formation.[3−6] Recently, attention has been focused on Cu nanoparticles due to their catalytic and electrocatalytic properties.[12−15] All the above properties depend on their size, size distribution, shape, and structure in addition to the interaction between the surface of the nanoparticle and the stabilizer. Control of these features is not trivial as Cu nanoparticle formation is extremely sensitive to reaction conditions.[16] In addition, the stability of Cu nanoparticles is an important issue as they undergo oxidation to Cu_2O or CuO[17,18] easily in air as well as in water.

There are several reports of wet-chemical synthesis of copper nanoparticles with a variety of approaches.[19] It is now well established that a microfluidic reactor process offers an alternate solution to traditional wet chemistry in order to control size and size-distribution of nanoparticles.[20−22] We have recently demonstrated that sulfobetaine-stabilized Pd nanoparticles with controlled size and narrower size distribution, in comparison with batch scale process, can be synthesized by using a microfluidic reactor.[22,23] Sulfobetaine-stabilized nanoparticles offer a possibility to prepare nano colloids in polar solvents. Prior to the development of the microfluidic process for the synthesis of Cu nanoparticles, we have investigated the classical batch process based on the chemistry (eqs 1 and 2) reported in the literature.[24]

$$C_{12}H_{25}N(CH_3)_2(C_3H_6\text{-}SO_3) + LiBEt_3H \rightarrow C_{12}H_{25}N(CH_3)_2(C_3H_6\text{-}SO_3)\cdot LiBEt_3H \quad (1)$$

$$2C_{12}H_{25}N(CH_3)_2(C_3H_6\text{-}SO_3)\cdot LiBEt_3H + CuC_2 \rightarrow Cu_{colloid}\cdot [C_{12}H_{25}N(CH_3)_2(C_3H_6\text{-}SO_3)]_2 + 2BEt_3 + 2LiCl + H_2 \quad (2)$$

Some of the technical challenges we have encountered during the synthesis using the classical batch process are (i) the copper(II) chloride ($CuCl_2$) and copper(I) chloride (CuCl) have a low solubility in tetrahydrofuran (THF) (<1 g/L at room temperature) leading to a slurry formation, at higher concentration (ii) separation of Cu nanoparticles free from the surfactant and salt impurities was found to be difficult leading to contamination with chloride ions forming copper oxide impurities as seen by XRD, and (iii) larger size Cu nanoparticles with broad size-distribution were obtained. The first two problems need to be addressed in order to translate the batch process into the microfluidic process. This translation will require greater detailed investigations into the factors affecting the formation of sulfobetaine-stabilized Cu nanoparticles. Even though there are several reports on the mechanistic investigations of the formation of nanoparticles in general,[25−27] very few of those reports pertain to Cu nanoparticle formation in solution phase[26,27] or on solid supports.[28] These studies suggest a multistep formation of Cu

[†] Louisiana State University.
[‡] Tulane University.

10.1021/jp044777g CCC: $30.25
Published on Web 04/22/2005

nanocolloids by reduction of copper(II) salts and revealed that the ligands may play an important role in the formation of intermediates.[26−28] However, the stabilizers used in these studies were non-zwitterionic and are different from sulfobetaines, the intermediates were not completely characterized, and the color changes were not monitored systematically possibly due to faster reaction rates in comparison with the formation of sulfobetaine-stabilized copper nanoparticles. More specifically, to the best of our knowledge, there is no report on the investigation of intermediates in the formation of sulfobetaine-stabilized copper nanoparticles. We have, therefore, carried out a detailed mechanistic investigation of the batch process for the formation of sulfobetaine-stabilized Cu nanoparticle using in situ UV−vis spectroscopy, XANES, and reaction calorimetry. The information obtained from the mechanistic investigations was utilized to develop a microfluidic process for the synthesis of copper nanoparticles. It is also important to note that while there is a large amount of literature on the use of differential scanning calorimetric investigation of nanoparticles for understanding phase transformations in solid nanoparticles,[29] there are very few literature reports on the use of in situ reaction calorimetry to investigate the formation of intermediates in solution phase during the wet-chemical synthesis of nanoparticles.[30] We report here, for the first time, reaction calorimetric investigations to understand the formation of intermediates during the synthesis of sulfobetaine-stabilized Cu nanoparticles. The ability to utilize intermediates formed during the synthesis of nanomaterials is a new approach for manipulating material synthesis at the nanometer scale and such an approach has not been reported so far. This new approach is likely to have an important role when considering magnetic nanoparticles such as cobalt where anisotropy and magnetization depend on structural and electronic properties.

Experimental Section

Batch Process. In a 250-mL three-necked round-bottomed flask equipped with a flow control inlet adapter, $CuCl_2$ (0.4735 g; 3.5 mmol) was loaded and the flask was evacuated completely. The flask was filled with nitrogen and the process of evacuation and refilling was carried out three times to ensure that the reaction flask was free from even trace amounts of oxygen. THF (25 mL) was added to the reaction flask under nitrogen. In a similar procedure, sulfobetaine (SB-12; 1.203 g, 3.5 mmol) was dissolved in 25 mL of THF under sonication and mixed with 7.0 mL of 1 M lithium hydrotriethylborate ($LiBEt_3H$)·THF solution. After the solution became clear, it was added into $CuCl_2$·THF solution dropwise over 30 min. After the addition, the reactants were stirred for another 30 min to ensure completion of the reaction followed by the addition of 10 mL of acetone to destroy the excess reducing agent. The Cu nanoparticles were allowed to settle down. The particles were separated, washed thoroughly with THF to remove physically bound surfactant, and dried under N_2 flow to obtain a fine red powder.

Experimental Setup for Reaction Calorimetry. $CuCl_2$ (6.67 g; 49.6 mmol of 99.999% purity) and anhydrous THF (352 g) were transferred to glass containers in a drybox under nitrogen atmosphere. Each container was removed from the drybox and its contents were transferred, under a nitrogen atmosphere, to the 1-L glass reactor connected to a Mettler-Toledo RC1 calorimeter. The $CuCl_2$ slurry was calibrated at 25°C to determine the overall heat transfer coefficient. During calibration, a fresh solution of SB-12 and $LiBEt_3H$ was prepared in a drybox under a nitrogen atmosphere. The solution was prepared by initially adding SB-12 (42.29 g; 126.0 mmol) to 220 g of anhydrous THF. To this slurry was added 249 mL of a 1.0 M solution of $LiBEt_3H$ in THF. This mixture produced a clear solution after 30−45 min of stirring. The entire contents of this solution was transferred to a clean and dry container. The container was removed from the drybox and connected to the suction of a diaphragm pump. Prior to feeding this SB-12/$LiBEt_3H$ solution, the entire length of the feed line was purged thoroughly with nitrogen to remove trace amounts of oxygen and moisture. A total of 304.5 g of SB-12/$LiBEt_3H$ solution (156.5 mmol of $LiBEt_3H$) was fed to the $CuCl_2$/THF slurry over a 30−45 min period. At the conclusion of the feed period, the mixture was stirred until no net heat generation was measured. Once heat generation ceased, the final slurry of copper nanoparticles was calibrated to determine the overall heat transfer coefficient. Then, acetone (15 mL) was added to the slurry to destroy the excess reducing agent and the reactor contents was transferred to a dry container under nitrogen atmosphere. A washing, filtration, and drying procedure similar to that described in the previous section was performed to isolate the copper nanoparticles. A total of three experiments were conducted. The overall material balance for each calorimetry experiment was in excess of 98%.

Microfluidic Reactor Process. The setup used for the microfluidic reactor process was described in ref 22. The reactant solutions had the same composition as used in the batch process. A gray blue clear solution was obtained when the SB-12 stabilized lithium hydrotriethylborate (Li[BEt_3H])·THF solution was added into the $CuCl_2$ slurry dropwise to reach a molar ratio of $CuCl_2$ to Li[BEt_3H] of about 0.75−0.83/1. The gray blue solution and the residual SB-12 stabilized lithium hydrotriethylborate (Li[BEt_3H])·THF solution were introduced into the microreactor at a flow rate required to finish the reaction in 30 min. The work-up procedure was similar to the case of a small batch process to obtain a fine red powder of Cu nanoparticles.

Characterization. The particle size, shape, and the size-distribution were characterized by using transmission electron microscopy (TEM 2010, 200KV, 0.23 nm, JEOL) by placing a drop of well-suspended Cu nanoparticles in ethanol on a carbon-coated gold TEM grid at room temperature and allowing the solution to evaporate. The SAED (Selected Area Electron Diffraction) was carried out with transmission electron microscopy together with the TEM images. The X-ray diffraction (XRD) experiments were conducted on a Bruker/Siemens D5000 automated powder X-ray diffractometer, using Cu $K\alpha_1$ radiation (λ = 1.540562Å) with Rietveld analysis software. XANES experiments were performed at the X-ray microprobe double crystal monochromator beamline equipped with a pair of plane Si(311) crystals at port 5A of the Center for Advanced Microstructures and Devices (CAMD) synchrotron radiation source at Louisiana State University.[31] The storage ring was operated at the electron beam energy of 1.3 GeV. The energy bandwidth for the excitation radiation was less than 2 eV over the range of energies examined. Spectra were background subtracted (linear background) and normalized at 8998.7 eV, using the standard procedures.[32,33] For the calibration of the energy scale of the monochromator, the Cu 1s energy was assigned to the first inflection point in the spectrum of a Cu foil (8979 eV). The in situ characterization of copper nanoparticle formation was carried out with XANES and UV/Vis (Thermo Spectronic, Genesys 10-5, Rochester, NY) spectroscopy at different Li[BEt_3H]:$CuCl_2$ molar ratios. The samples for in situ characterization were prepared by adding the reducing

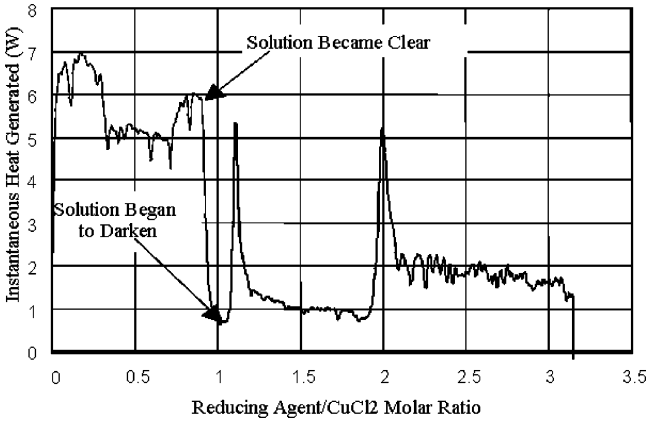

Figure 1. Heat generated as a function of the ratio of reducing agent ($Li[B(C_2H_5)_3H$) to $CuCl_2$ during Cu nanoparticle formation with a mole ratio of $Li[B(C_2H_5)_3H$/SB-12 = 2:1.

agent THF solution (SB-12:Li[BEt_3H]) to the $CuCl_2$·THF solution under stirring. The XANES spectra were collected immediately at room temperature after the Li[BEt_3H]:$CuCl_2$ solution was loaded into a sealed cell with a Kapton film window. The samples for UV/vis were prepared in THF and the optical absorption spectra were collected from 200 to 900 nm at room temperature.

Results and Discussion

In Situ Reaction Calorimetry. The reaction calorimetry data provide information on the heat of the reaction, presence of any stable intermediates, optimum ratio of reactants, and concentration. To the best of our knowledge reaction calorimetry studies on nanoparticle formation in general[30] and copper nanoparticles in particular have not been reported previously. Chemical control of the synthesis at a nanometer scale is possible through understanding and manipulation of intermediates formed during the nanomaterial preparation. Such an ability will pave the way for obtaining better control over crystal structure, shape, size, and size-distribution of nanomaterials. We believe that reaction calorimetry will play an important role in understanding the mechanistic aspects of nanomaterial formation leading to the preparation of newer types of materials. We used in situ reaction calorimetry to measure the overall enthalpy change and monitor the evolution of associated intermediates during the formation of sulfobetaine-stabilized copper nanoparticle. Figure 1 provides the instantaneous heat generation observed during the sulfobetaine-stabilized Cu nanoparticle synthesis as a function of the molar ratio of reducing agent fed to the $CuCl_2$ initially charged in the reactor. The molar ratio of the stabilizing agent to reducing agent was maintained at 1:2. Due to its low solubility in THF, $CuCl_2$ was originally slurry in the reactor. The initial high heat generation rate was primarily the result of a rapid reaction between the copper(II) chloride slurry and the reducing agent. Once sufficient reducing agent had been fed (approximately 0.9:1 molar ratio of reducing agent to initial $CuCl_2$), the solution became clear for a short period. At a 1:1 molar ratio of reducing agent fed to initial $CuCl_2$, the solution began to darken and a peak was observed. While this peak is most likely the result of a nucleation or phase change event, the state of the nanoparticles formed could not be determined solely by calorimetry. Of additional interest is the fact that only one-half of the reducing agent required to completely reduce all $CuCl_2$ present had been added at this point when these visual and thermal observations were made. One might, therefore, postulate the formation of a Cu^+ intermediate.

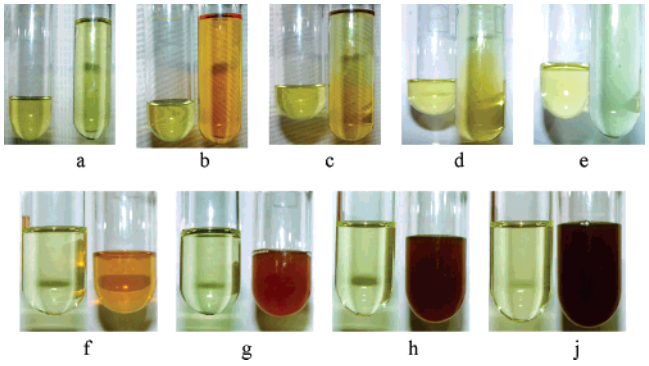

Figure 2. Color changes at different reducing agent:$CuCl_2$ molar ratios. All left samples are the control $CuCl_2$·THF solution. (a) $CuCl_2$·THF solution; (b) molar ratio of reducing agent:$CuCl_2$ = 0.2:1; (c and d) the honey yellow complex solution is changing to gray blue Cu^+ complex solution by diffusion of reducing agent from top to bottom at slow addition of the reducing agent; the final stable gray blue Cu^+ complex solution with reducing agent:$CuCl_2$ = 0.83:1; (f) reducing agent:$CuCl_2$ = 1:1; (g) reducing agent:$CuCl_2$ = 1.25:1; (h) reducing agent:$CuCl_2$ = 1.5:1; (j) reducing agent:$CuCl_2$ = 2:1.

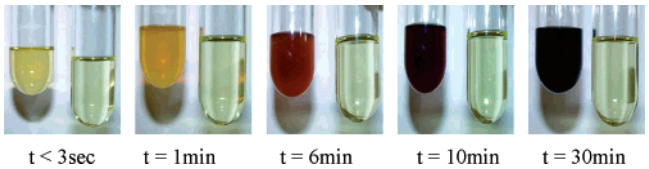

Figure 3. Time dependent color change at the mole ratio of reducing agent:$CuCl_2$ of 1.5:1 by quick addition of the reducing agent solution. All right samples are $CuCl_2$·THF solution for comparison.

The occurrence of a second peak in the instantaneous heat generation was not accompanied by a visual change in the solution. This peak could be the result of a second nucleation or phase changing event. Based on the overall reaction (eq 2) the measured heat of the reaction from this study is -40.0 ± 0.22 kcal/gmol of $CuCl_2$. Note that this overall heat of reaction neglects heat of solution contributions from any of the species in THF. To verify the presence of intermediate Cu^+ species, both UV−vis and XANES spectroscopy analysis were carried out. While higher $CuCl_2$ concentrations were required to determine an accurate heat of reaction, both spectroscopy analyses were conducted with saturated solutions in THF.

UV/Vis Spectroscopy. Visible color changes during the course of addition of the reducing agent to the $CuCl_2$ provided possible evidence for the formation of a stable Cu^+ complex. Previously reported studies on the Cu nanoparticle formation based on UV/vis spectral analysis revealed that the peak position of the plasmon resonance was ligand-dependent.[25e,27] It appears that only when the particle size reaches a minimum size that the plasmon resonance from the Cu nanoparticles was detectable by UV/vis spectroscopy.[25e] There is no report on systematic examination of visible color changes during the formation of copper nanoparticles. As shown in Figure 2, the color of the $CuCl_2$ solution changed from yellow to orange, then to gray blue when the molar ratio of the reducing agent to Cu^{2+} (the ratio of SB-12 to reducing agent was kept at 2:1) reached 0.75−0.83:1. The gray blue solution remained unchanged if left undisturbed at this stage over a period of 12 h. However, with further addition of the reducing agent, the color changed to red and then, finally, to darker red. When all the reducing agent was added at once to the $CuCl_2$ (the ratio of reducing agent to $CuCl_2$ was 1.5:1), similar changes in color were observed with respect to time as shown in Figure 3 and the reaction solution became completely dark red within 30 min. The gray-blue color

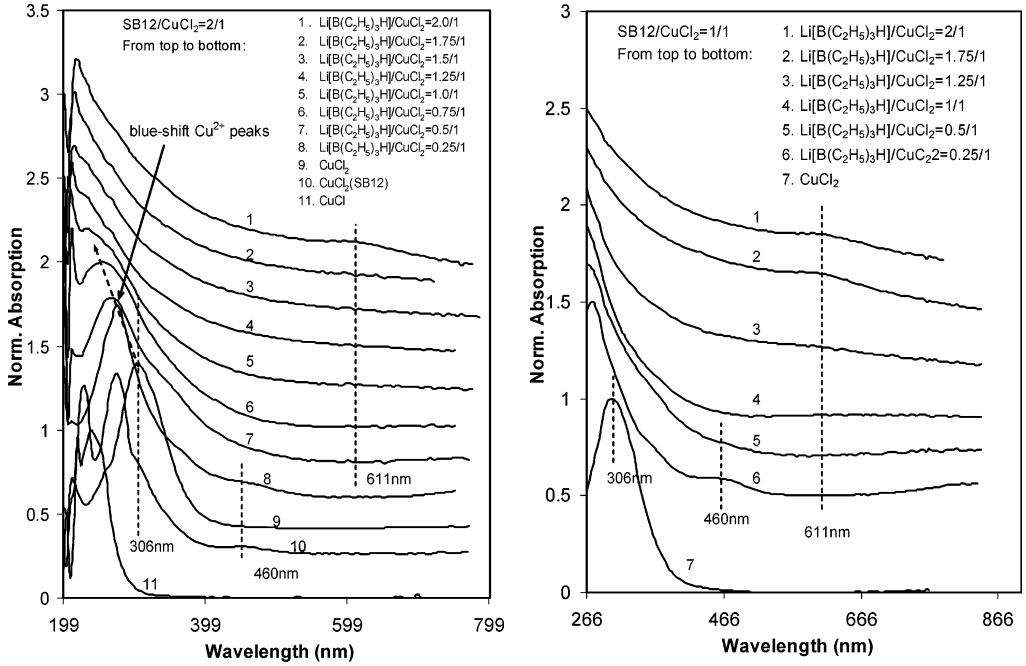

Figure 4. UV/vis spectra taken at different stages of Cu nanoparticle formation at different SB-12:Li[$B(C_2H_5)_3H$]:Cu^{2+} molar ratios. Peaks at 306, 460, and 611 nm represent $CuCl_2$ in THF solution, the sulfobetaine−Cu(II) complex, and the formation of Cu nanocolloids, respectively. (a) Mole ratio of SB-12/Li[$B(C_2H_5)_3H$] = 1/1; final mole ratio of $CuCl_2$/Li[$B(C_2H_5)_3H$]/SB-12 = 1/2/2. (b) Mole ratio of SB-12/Li[$B(C_2H_5)_3H$] = 1/2; final mole ratio of $CuCl_2$/Li[$B(C_2H_5)_3H$]/SB-12 = 1/2/1.

could not be stabilized. Similarly, when the molar ratio of SB-12 to reducing agent was less than 2, the gray-blue color was not stable. Monitoring of the systematic color changes with variation in the molar ratio of reducing agent to $CuCl_2$ was also carried out with UV/vis spectroscopy. As seen from Figure 4a, the absorbance for free Cu^{2+} at 306 nm (∼290 nm for Cu(II):SB-12 complex) was blue-shifted with the addition of the reducing agent and closely resembled the reference CuCl spectrum when the molar ratio of reducing agent to Cu^{2+} approached 1:1. The absorption peak at 460 nm, typical for Cu^{2+}:SB-12 complex, also disappeared at this stage. The absorption peak due to plasmon resonance, typical for copper colloids at 611 nm, did not appear until the molar ratio of reducing agent to Cu^{2+} reached 2:1, indicating that only when the concentration of the cluster or the size of the Cu colloids reached a critical value was the plasmon resonance peak for Cu nanoparticles detected in the UV/vis spectrum. However, it is interesting to note that when the molar ratio of SB-12 to $CuCl_2$ was kept at 1:1, the plasmon resonance peak appears at a lower molar ratio of reducing agent to $CuCl_2$ (Figure 4b). Both from the visible color change as well as from the UV/vis spectral analysis, it can be concluded that a stable Cu^+ complex can be obtained by controlling the amounts of stabilizing agent and reducing agent relative to $CuCl_2$.

In situ X-ray Absorption Near Edge Structure Spectroscopy. XANES (X-ray absorption near edge structure) has proven to be a powerful tool to investigate transition metal colloids in order to obtain a direct insight into the geometric and electronic structure of an absorbing metallic center.[34,35] We have, therefore, made an attempt to understand the changes at the copper center with increase in molar ratio of reducing agent to $CuCl_2$ maintaining the reducing agent to SB-12 molar ratio at 2:1. Various sulfobetaine−copper complexes formed under different ratios of reducing agent and SB-12 are described below. In the absence of reference samples, it was not possible to conclusively prove the structures of these complexes. However, attempts were made to characterize them reasonably well by comparing the XANES spectral data of similar compounds obtained from the literature.

Tetracoordinated Sulfobetaine−Cu(II) Complex. When the stabilizing agent SB-12 was added to $CuCl_2$ in THF, a tetracoordinated complex was formed (Figure 5, 1) with a pre-edge feature(A′and B′) and shape resonance (C′ and D′) similar to the XANES spectrum of $[N(octyl)_4]_2[CuCl_2Br_2]$ [27] (Figure 5-2, see Figure 2b in ref 27). The minute differences in the position of peaks C′ and D′ in the two spectra could be attributed to differences in the nature of the ligands. Although the plasmon resonance position of the $CuCl_2$−SB-12 complex in THF (see curve 10 in the UV/vis spectra of Figure 4) is different from that of $[N(octyl)_4]_2[CuCl_2Br_2]$ in toluene described by Rothe et al.,[27] the XANES of the $CuCl_2$−SB-12 complex (Figures 5-1) displayed the same characteristic structures of a divalent Cu complex as $[N(octyl)_4]_2[CuCl_2Br_2]$, which was quite similar to the spectrum of divalent Cu in square-planar $[NEt_4]_2CuCl_4$.[27] Though the tetracoordinated complex in our case is likely to be square planar, it was not possible to rule out tetragonal architecture.

Linear Sulfobetaine−Cu(I) Complex. On increasing the ratio of reducing agent to $CuCl_2$ near to the stoichiometric ratio to reduce Cu^{2+} to Cu^+ completely, a blue-gray complex was obtained. (Figures 5-4). Unlike the unstable Cu^+ complex (yellow solution) reported in the case of $[N(octyl)_4]_2[CuCl_2Br_2]$, the blue-gray sulfobetaine−Cu(I) complex we have obtained was stable. The Cu K-edge XANES spectrum taken at this stage of the reaction revealed an intense pre-edge peak at 8982.3 eV (Figure 5-4, A) and peaks at 8991 eV (Figure 5-4, B) and at 9011 eV (Figure 5-4, C). The XANES spectrum was compared to the reference XANES spectra of Cu(I) complexes from the literature.[27,28,35] The reference spectra are given in Figure 5 for linear Cu(I) complex and in Figure 6 for tricoordinated Cu(I) complex. The peak positions and ratios of the pre-edge peak to the first unresolved peak for the sulfobe-

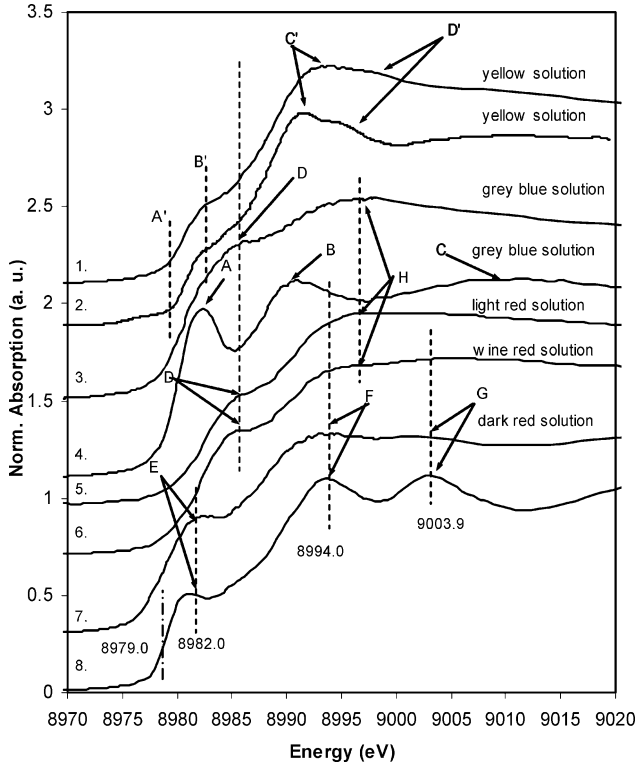

Figure 5. In-situ Cu K-edge XANES spectra at different stages of Cu colloid formation. From top to bottom: (1) $CuCl_2$·(SB12) in THF (offset 2.1); (2) $[N(octyl)_4][CuCl_2Br_2]$ in toluene (ref 26, Figure 2b) (offset 1.8); (3) CuCl (SB12) in THF (offset 1.5); (4) $CuCl_2$/Li[$B(C_2H_5)_3H$] = 1/0.75 (offset 1.1); (5) $CuCl_2$/Li[$B(C_2H_5)_3H$] = 1/1 (offset 0.95); (6) $CuCl_2$/Li[$B(C_2H_5)_3H$] = 1/1.5 (offset 0.7); (7) $CuCl_2$ /Li[$B(C_2H_5)_3H$] = 1/2 (offset 0.3); (8) fcc Cu foil.

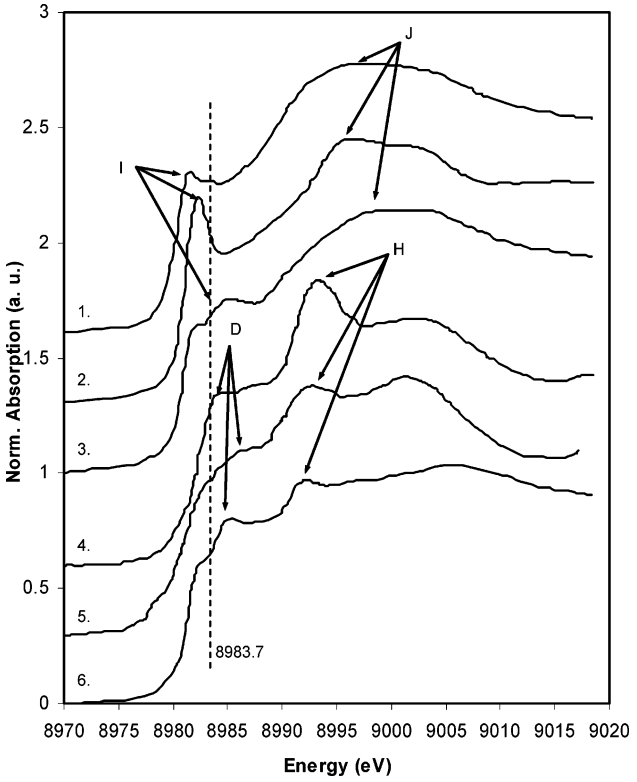

Figure 6. Reference XANES spectra of tricoordinated and tetracoordinated Cu(I) complexes: (1) $Cu_2ISOIM(t\text{-}Bu)_2(pz)$ (offset 1.6); (2) $Cu(pze)BF_4$ (offset 1.3); (3) $[Cu_2(mxyN_6)](BF_4)_2$ (offset 1.0); (4) $[Cu(py)_4]ClO_4$ (offset 0.6); (5) Cu(tepa)BPh_4 (offset 0.3); (6) Cu(2,5-DTH)$_2ClO_4$.

taine−Cu(I) complexes and reference Cu(I) complexes are summarized in Table 1.

The XANES spectrum of sulfobetaine−Cu(I) complex in Figure 5-4 appears to be more similar to a linear Cu(I) complex since its pre-edge at 8982.3 eV is closer to the referred Cu(I) complexes (8982.5−8982.7 eV). Also the ratio of the first unresolved peak to the pre-edge peak (0.87) is closer to those for the linear Cu(I) complexes (0.92 for $[Cu(Br)_2]^-$, 1.0 for $[Cu(xypz)]_2(BF_4)_2$, and 0.85 for $[Cu(EDTB)]_2(ClO_4)_2$) than to those of the tricoordinated Cu(I) complexes and the tetracoordinated Cu(I) complexes (see their values in Table 1). The XANES spectra of tricoordinated complexes (Figure 6-1, -2, and -3) and tetracoordinated complexes (Figure 6-4, -5, and -6) exhibit a pre-edge feature at a lower energy (Figure 6, points I and D) than in the linear complexes (Figure 5, point A).[28] Hence, the as-formed blue-gray sulfobetaine−Cu complex is likely to be mainly a linear Cu(I) complex. The pre-edge peak at 8982.0 eV could be attributed to the transition of an electron from the 1s (Cu) to the $4p_{x,y}$ (Cu) states.[28,35] Since the ratio of the superhydride to Cu^{2+} was closer but slightly less than the stoichiometric ratio (1:1) for complete formation of Cu^+ complexes, one could not rule out completely the presence of smaller amounts of sulfobetaine−Cu(II) complex.

When CuCl was directly complexed with a sufficient amount of SB-12 in THF, once again a gray-blue complex was obtained. However, the XANES spectrum of this complex (Figure 5-3) revealed that the complex is more likely to be a tetracoordinated complex, with almost the same pre-edge feature (8985.7 eV) and ratio of the first unresolved peak to the pre-edge peak (0.80) as in the case of the reference XANES spectrum of tetracoordinated Cu(2,5DTH)$_2ClO_4$ (8985.3 eV and 0.82). Comparison

TABLE 1: Peak Positions and Ratios of the Pre-edge Peak to the First Unresolved Peak for the Sulfobetaine Copper Complexes and Reference Cu(I) Complexes[27,35]

compds		pre-edge (eV)	first unresolved peak (eV)	ratio of first unresolved peak to pre-edge peak
spectrum no. of sulfobetaine-stabilized Cu complexes	Figure 5-3	8985.7	8994.6	0.80
	Figure 5-4	8982.3	8991.0	0.87
	Figure 5-5	8985.7	8996.2	0.59
	Figure 5-6	8984.7	8994.2	0.67
linear	$[Cu(Br)_2]^-$	8982.5	8986.5	0.92
	$[Cu(xypz)]_2(BF_4)_2$	8982.7	8998.7	1.0
	$[Cu(EDTB)]_2(ClO_4)_2$	8982.5	8994.7	0.85
tricoordinated	$Cu_2ISOIM(t\text{-}Bu)_2(pz)$	8981.8	8996.0	0.6
	$Cu(pze)BF_4$	8982.6	8996.4	0.76
	$[Cu_2(mxyN_6)](BF_4)_2$	8984.9	8998.2	0.67
tetracoordinated	$[Cu(py)_4](ClO_4)$	8985.0	8993.6	0.61
	$Cu(tepa)BPh_4$	8986.2	8992.8	0.74
	$Cu(2,5\text{-}DTH)_2ClO_4$	8985.3	8992.5	0.82

of the pre-edge feature, the first unresolved peak and the ratio of the first unresolved peak to the pre-edge peak with those of the linear, tricoordinated, and tetracoordinated Cu(I) complex (Table 1) also confirms this assignment. Unlike the 2-coordinated linear complex but similar to the tricoordinate complex, a much reduced intensity at 8985.7 eV in the case of CuCl−SB12 in THF (Figure 5-3) represented the transition of an electron from 1s to $4p_i$ ($i = x, y, z$).[28,35]

When the ratio of Li[Et_3BH]-SB12 to Cu^{2+} was no less than 1/1 or the ratio of SB12 to Cu^{2+} was lower than 2/1, the gray-blue Cu^+ complex formed became unstable and changed to a reddish colored solution within 5 min. A light red solution was formed at a ratio of Li[Et_3BH] to Cu^{2+} of about 1/1. The

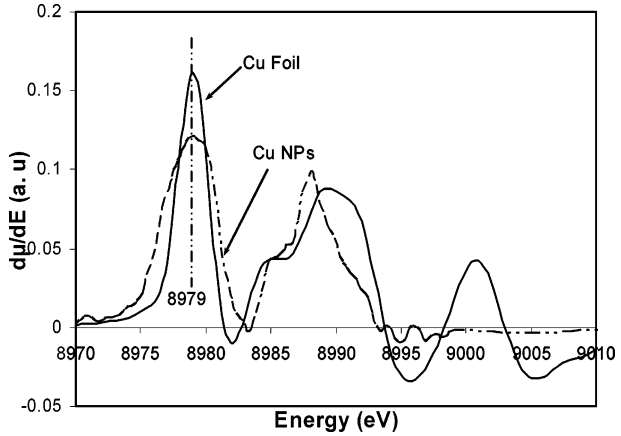

Figure 7. First derivatives of the spectra of Cu nanoparticles showing a similar pre-edge feature (the same first inflection point at 8979 eV) and the shape resonance as that of the fcc Cu foil.

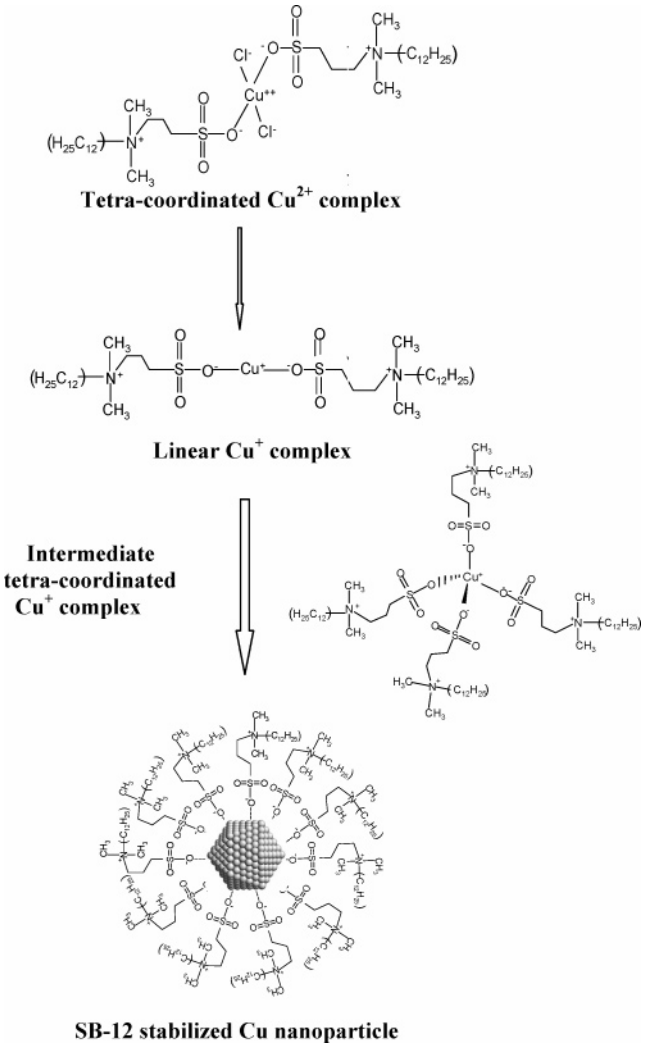

Figure 8. Proposed steps during Cu nanoparticle formation: The tetra-coordinated sulfobetaine Cu^{2+} complex changes to a linear Cu^{+} complex which further changes to the final product, SB-12 stabilized Cu nanoparticle, possibly through an intermediate tetra-coordinated Cu^{+} complex.

XANES spectrum obtained at this stage is given in Figure 5-5. Since the sulfobetain−Cu^{+} complex usually showed blue-gray color in THF, the reddish color could be attributed to the formation of Cu(0)−SB12 clusters and/or Cu^{2+} complexes via the disproportionation of Cu^{+} (eq 3) when the Cu^{+} concentration

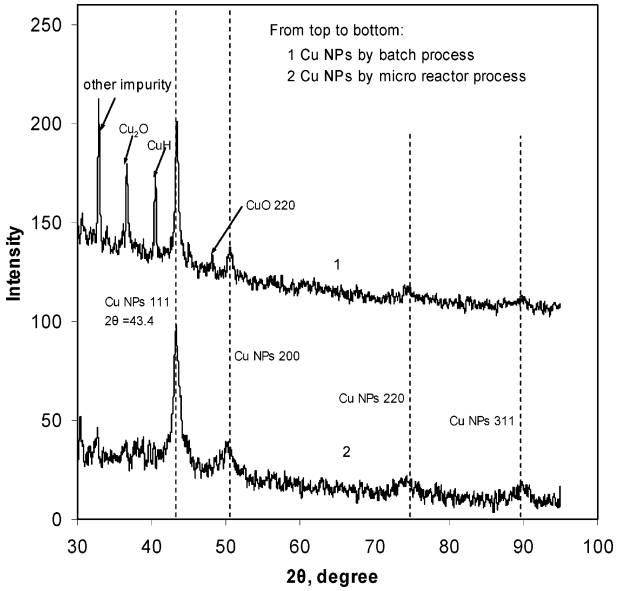

Figure 9. XRD patterns for the Cu nanoparticles synthesized by the two processes.

increased to a value that could be stabilized in the solution condition.[34] The time-dependent color variation of the as-formed complex solution after the ratio of Li[Et_3BH] to Cu^{2+} was no more than 1/1 indicated that it is more likely to be the disproportionation of Cu^{+} (Figure 3).

$$2Cu^{+} \rightleftharpoons Cu^{2+} + Cu_{clusters} \qquad (3)$$

Due to similarities in the pre-edge feature (8985.7 eV, Figure 5-5, point D) and the shape resonance (with a ratio of the first unresolved peak to the pre-edge peak about 0.59) of the XANES spectra of the as-formed light-red solution (Figure 5-5) and the reference tetracoordinated Cu(I) complexes, particularly as [Cu(py)](ClO_4) (8985.0 eV and 0.61), one could infer that the light-red solution was mainly due to the formation of a tetracoordinated Cu(I) complex. It is also to be noted that the XANES feature of Cu^{2+} and the Cu clusters are absent likely due to the undetectable concentration of Cu^{2+} and low disproportionation constant.[34] In the formation of Cu nanoparticles investigated with UV−vis spectral analysis, it was also observed that the intensity of the absorption peak due to Cu^{2+} reduces quickly even before the ratio of Li[Et_3BH] to Cu^{2+} reached the stoichiometric ratio to form Cu^{+} completely (Figure 4) and the plasmon resonance of Cu nanoparticles did not appear until the Cu clusters grew to a threshold size. The formation of the Cu clusters is likely to release more SB12 into the solution enhancing the possibility for formation of tetracoordinated Cu(I) complexes from the linear Cu(I) complexes. The situation can be compared to the case where tetracoordinated Cu(I) complex was obtained directly by mixing sufficient SB12 with CuCl.

SB-12 Stabilized Cu Nanoparticles. With continued addition of Li[Et_3BH]-SB12 into the Cu(I) complex/Cu^{2+} THF solution to increase the ratio of Li[Et_3BH] to Cu^{2+} more than 1/1, the Cu^{+} and/or Cu^{2+} could be directly reduced to Cu atoms leading to the formation of Cu clusters. When the molar ratio of Li[Et_3BH] to Cu^{2+} was about 1.5/1, the XANES spectrum of this reaction solution (Figures 5 and 6) showed a very similar pre-edge feature and shape resonance as the XANES spectrum of the reaction mixture at a molar ratio of Li[Et_3BH] to Cu^{2+} of

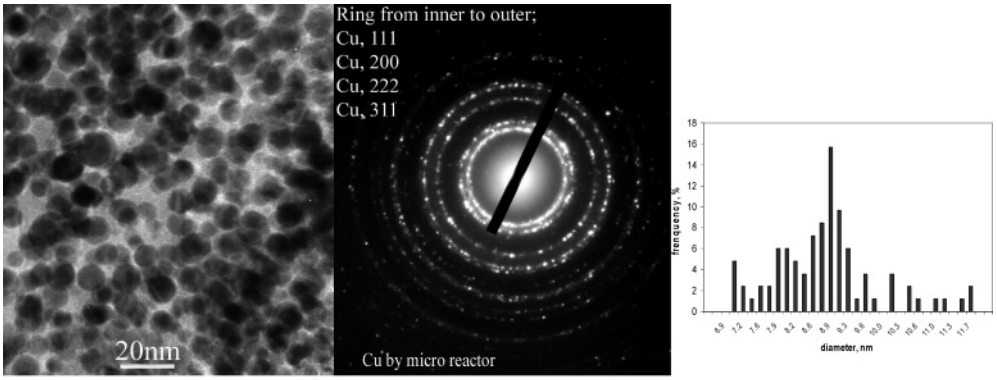

A: by micro reactor process (%STDEV=20%)

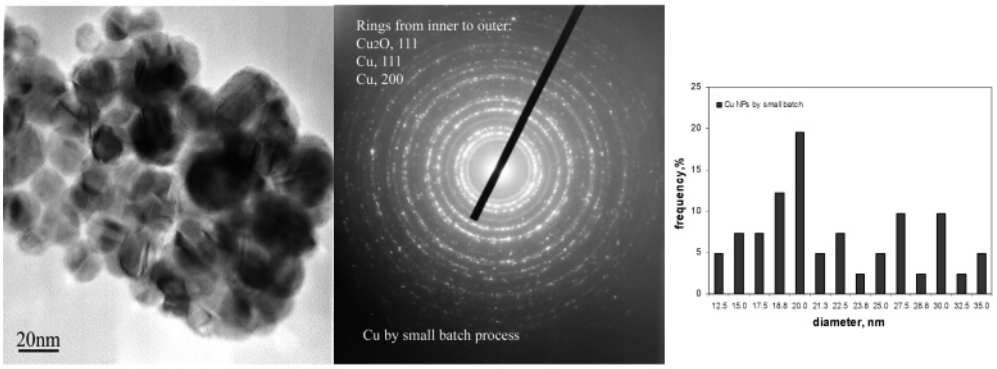

B: by batch process (100mL, %STDEV=26%)

Figure 10. Cu nanoparticles synthesized by the two processes (from left to right: TEM image, SAED pattern, and particle size distribution).

about 1/1. The rate of formation of Cu atoms and the growth rate of Cu clusters increased rapidly with the increase in concentration of the reducing agent, indicated by the color change of the reaction solution from light red to wine red. As can be observed from the XANES spectrum, the pre-edge peak and the first unresolved peak shifted to a low energy (Table 1 and Figures 5 and 6). Another resonance peak at 9003.7 eV, usually appearing in the XANES spectrum of Cu nanoparticles (Figure 5-7) or Cu foil (Figure 5-8), appeared clearly.

When the ratio of $Li[Et_3BH]$ to Cu^{2+} was maintained at about 2/1 for some time (~10−30 min), the XANES spectrum at this stage clearly showed similar pre-edge features and shape resonances as that of fcc Cu foil. The shoulder positions (peak D in Figure 5-5) at 8985.7 eV (representing the tetracoordinated Cu^+ state) completely shifted to 8982.7 eV (representing the Cu^0 state, Figure 5-7, E). From the derivatives of the spectra plotted in Figure 7, the position of the first inflection point coincided with that of the standard fcc Cu foil (8979 eV). The shoulder peak and the distinct peaks at 8993 eV (Figure 5-7 and -8, point F), 9003.7 eV (Figure 5-7 and -8, point G) indicated that the final Cu nanocolloids have fcc crystal structure. At low SB-12 to $CuCl_2$ mole ratios, it was observed that the gray-blue linear Cu^+ complex was not stable and changes quickly to the tetracoordinated Cu^+ complex and then to the Cu^0 state. That was one of the reasons that the peak at 611 nm representing Cu nanocolloid formation appeared much earlier in the UV/vis spectrum at lower SB-12 to $CuCl_2$ molar ratios. When the $Li[BEt_3H]$/SB-12 solution was added quickly, the situation was similar to that observed when lower SB-12 to $CuCl_2$ mole ratios were employed. This indicates that the formation of the linear Cu^+ complex was sensitive to the reaction rate of Cu^{2+} reduction controlled by both the surfactant SB-12 concentration and the addition rate of the reducing agent. The reason for obtaining a stable linear sulfobetaine−Cu^+ complex at the stoichiometric ratio of reducing agent and $CuCl_2$ may be due to low disproportionation constant for the linear Cu^+ complex resulting in its disproportionation to Cu^0 and Cu^{2+}. This is similar to the case of Cu^+ in liquid NH_3, particularly in solutions with sufficient Cu^{2+}.[34] Both the visible color changes of the reaction solutions at different reducing agent to $CuCl_2$ molar ratios and the XANES spectra indicate that the zerovalent Cu was formed only after the reducing agent:$CuCl_2$ molar ratio exceeds (0.75−0.83)/1. On the basis of the understanding gained from the above investigations, it was possible to envisage the presence of a stable and homogeneous SB-12:Cu^+ complex as an intermediate in a number of steps leading to the Cu nanoparticle formation as shown in Figure 8. In the first step, the tetracoordinated sulfobetaine−Cu(II) complex is reduced to the linear Cu(I) complex. When the molar ratio of reducing agent to $CuCl_2$ is greater than 1:1, tetracoordinated Cu(I) complex is formed by coordinating with two more SB12 molecules released due to the formation of Cu^0 clusters through reduction of linear sulfobetaine−Cu(I) complex. However, it is not possible to postulate if the tetracoordinate Cu^+ complex is an intermediate between the linear Cu^+ complex and the Cu^0 or if the Cu^0 can be obtained directly from the Cu^+ linear complex. A more detailed investigation is required to understand the formation of the Cu^+ tetracoordinated complex.

Since a stable and homogeneous sulfobetaine−Cu(I) complex solution can be obtained, the microreactor process was designed to utilize this as one of the reactants as our attempts to obtain a similar complex directly using Cu(I)Cl and SB-12 were

TABLE 2: Properties of Cu Nanoparticles Synthesized by the Two Processes

sample name	d_n,[a] nm	% STDEV	$\bar{a}_i$,[b] Å	fwhm01,[c] deg
Cu by small batch	22.5	26	3.609	0.45
Cu by microreactor	8.9	20	3.614	0.85
bulk Cu[36]			3.6148	

[a] d_n: the number mean diameter. [b] $\bar{a}_i$: the lattice parameter calculated from XRD pattern. [c] fwhm01: the full-width at half-maximum intensity for the most intensive peak.

unsuccessful. Therefore, first, a stable soluble Cu^+ complex was prepared by adding reducing agent solution containing SB-12 into the bulk $CuCl_2$ solution slowly to obtain the gray-blue sulfobetaine−Cu(I) complex. The Cu^+ solution and the remaining reducing agent were introduced separately through two inlets into the microreactor to react together. After the completion of the reaction, acetone was introduced into the product flask to quench the reaction and the Cu nanoparticles settled down from the colloid solution quickly. The impurities such as salts and the surfactant could now be easily washed out. The XRD spectrum for the Cu nanoparticles is given in Figure 9. Figure 10 shows the size and size-distribution of Cu nanoparticles synthesized by the two methods based on TEM images. The physical properties of the sulfobetaine-stabilized Cu nanoparticles are summarized in Table 2. The Cu nanoparticles synthesized by the microfluidic process had typical fcc structure unlike the case of palladium nanoparticles reported in ref 22. Also, they have a closer packing of atoms than the bulk Cu (near or smaller lattice parameter $\bar{a}_i$).[36] TEM images and data in Table 2 show that Cu nanoparticles synthesized by the microreactor process have a smaller size and narrower size-distribution in comparison with those produced by the conventional batch process.

The XRD spectrum of the Cu nanoparticles from the microreactor process (Figure 9 (No. 2)) shows no Cu_2O peak, indicating that Cu nanoparticles were not easily oxidized unlike the Cu nanoparticles synthesized from the batch process. The Cu nanoparticles also had smaller size and narrower size-distribution but similar fcc crystal structure in comparison with those obtained from the batch process. The SAED pattern (Figure 10) of the Cu nanoparticles synthesized by the microreactor process also showed no Cu_2O impurities.

Conclusions

Stable and water-soluble sulfobetaine−Cu(I) complex can be formed in THF solution by using 3-(*N*,*N*-dimethyldodecylammonia)propanesulfonate as a stabilizer during the Cu nanocolloid formation from $CuCl_2$•THF solution as indicated by the in situ XANES, UV−vis, and reaction calorimetry investigations. The Cu^+ complex changes from a linear complex to a tetracoordinated complex when the ratio of reducing agent to $CuCl_2$ is more than one. The stability of the linear Cu^+ complex was found to be sensitive to the addition rate of the reducing agent and the concentration of the stabilizer. Cu nanoparticles with narrower size-distribution and a smaller size could be synthesized by using sulfobetaine−Cu(I) complex as the starting material in the microreactor process in comparison with those obtained by the conventional batch process with $CuCl_2$. The Cu nanoparticles obtained from the microreactor process were also found to be more stable to oxidation.

Acknowledgment. This work was supported by grants from NSF-EPSCoR (Grant No. NSF/LEQSF (2001-04) RII-03) through the Louisiana Board of Regents. The authors thank Dr. J. Jiang of the Mechanical Engineering Department of LSU for the use of TEM, Dr. Amitava Roy in assisting with generation of comparative XANES spectra from the literature, Dr. W Leblanc of the Department of Geology for the use of XRD, and F. W. Orihuela for performing the reaction calorimetry experiments. Authors are also grateful to the reviewers for valuable suggestions.

References and Notes

(1) Puntes, V. F.; Krishnan, K. M.; Alivisatos, A. P. *Science* **2001**, *291*, 2115.

(2) (a) Song, Y.; Doomes, E.; Guo, Z.; Kumar, C. Hormes, J. Phase-Controlled Synthesis of Cobalt Nanoparticles Using a Microfluidic Reactor, 2004 MRS Fall Meeting, Nov 29−Dec 3, 2004. (b) Diana, F. S.; Lee, S.-H.; Petroff, P. M.; Kramer, E. J. *Nano Lett.* **2003**, *3*, 891.

(3) Wu, M.-L.; Chen, D.-H.; Huang, T.-C. *Chem. Mater.* **2001**, *13*, 599.

(4) Jana, N. R.; Wang, Zh. L.; Sau, T. K.; Pal, T. *Curr. Sci.* **2002**, *19*, 1367.

(5) Kim, F.; Song J. H.; Yang, P. *J. Am. Chem. Soc.* **2002**, *124*, 14316.

(6) Jana, N. R.; Gearheart, L.; Murphy, C. J. *Chem. Commun.* **2001**, 617.

(7) Liu, X.; Cai, W.; Bi, H. *J. Mater. Res.* **2002**, *17*, 1125.

(8) Huang, C.; Yang, C. Z. *Appl. Phys. Lett.* **1999**, *74*, 1692.

(9) Akamatsu, K.; Deki, S. *J. Mater. Chem.* **1997**, *7*, 1773.

(10) Kogiso, M.; Yoshida, K.; Yase, K.; Shimizu, T. *Chem. Commun.* **2002**, 2492.

(11) Eastman, J. A.; Choi, S. U. S.; Li, S.; Yu, W.; Thompson, L. *J. Appl. Phys. Lett.* **2001**, *78*, 718.

(12) Zhao, M.; Sun, L.; Crooks, R. M. *J. Am. Chem. Soc.* **1998**, *120*, 4877.

(13) Shim, I.-W.; Noh, W.-T.; Kwon, J.; Cho, J. Y.; Kim, K.-S.; Kang, D. H. *Bull. Korean Chem. Soc.* **2002**, *23*, 563.

(14) Petranovskii, P. V.; Gurin, S. V.; Bogdanchikova, E. N.; Phatanasri, S.; Praserthdam, P. *Proceedings of the SPIE 4806*; Lakhtakia, A., Dewar, G., McCall, M. W., Eds.; Complex Mediums III: Beyond Linear Isotropic Dielectrics; SPIE Publications: Bellingham, WA, June 2002; pp 233−239.

(15) Pestryakov, A. N.; Petranovskii, V. P.; Kryazhov, A.; Ozhereliev, O.; Pfander, N.; Knop-Geri *Chem. Phys. Lett.* **2004**, *385*, 173.

(16) (a) Hu, W.; Matsumura, M.; Furukawa, K.; Torimitsu, K. *J. Phys. Chem.* B **2004**, *108* (35), 13116. (b) Huang, C.; Yang, C. Z. *Appl. Phys. Lett.* **1999**, *74* (12), 1692. (c) Chen, T.-Y.; Chen, S.-F.; Sheu, H.-S.; Yeh, C.-S. *J. Phys. Chem. B* **2002**, *106* (38), 9717. (d) Chen, S.; Sommers, J. M. *J. Phys. Chem. B* **2001**, *105* (37), 8816.

(17) Kim, J. H.; Germer, T. A.; Mulholland, G. W.; Ehrman, S. H. *Adv. Mater.* **2002**, *14*, 518.

(18) Choi, H. C.; Jung, Y. M.; Kim, S. B. *Intl. J. Nanosci.* **2002**, *1*, 443.

(19) (a) Zhu, H.-T.; Zhang, C.-Y.; Yin, Y.-S. *J. Cryst. Growth* **2004**, *270* (3−4), 722. (b) Kitchens, C. L.; Roberts, C. B. *Ind. Eng. Chem. Res.* **2004**, *43* (19), 6070. (c) Schmittel, M.; Kalsani, V.; Kienle, L. *Chem. Commun.* **2004**, *13*, 1534.

(20) Edel, J. B.; Fortt, R. J.; deMello, C.; deMello, A. *J. Chem. Commun.* **2002**, 1136.

(21) Chan, E. M.; Mathies, R. A.; Alivisatos, A. P. *Nano Lett.* **2003**, *3*, 199.

(22) Song, Y.; Kumar, C. S. S. R.; Hormes, J. *J. Nanosci. Nanotechol.* **2004**, *4*, 88.

(23) Song, Y.; Kumar, C. S. S. R.; Hormes, J. *J. Micromech. Microeng.* **2004**, *14*, 932.

(24) Bonnemann, H.; Braun, G.; Brijoux, W.; Brinkmann, R.; Tilling, A.; Seevogel, K.; Siepen, K. *J. Organomet. Chem.* **1996**, *520*, 143.

(25) (a) Rodriguez-Sanchez, M. L.; Rodriguez, M. J.; Blanco, M. C.; Rivas, J.; Lopez-Quintela, M. A. *J. Phys. Chem. B* **2005**, *109* (3), 1183−1191. (b) Weigle, J. C.; Luhrs, C. C.; Chen, C. K.; Perry, W. L.; Mang, J. T.; Nemer, M. B.; Lopez, G. P.; Phillips, J. *J. Phys. Chem. B* **2004**, *108* (48), 18601−18607. (c) Wong, H.-W.; Li, X.; Swihart, M. T.; Broadbelt, L. J. *J. Phys. Chem. A* **2004**, *108* (46), 10122. (d) Ojo, C.; Blanco, M. C.; Lopez-Quintela, M. A. *Langmuir* **1998**, *14* (24), 6835−6839. (e) Murakata, T.; Higashi Y.; Yasui. N.; Higuchi, T.; Sato S. *J. Chem. Eng. Jpn.* **2002**, *35* (12), 1270−1276.

(26) (a) Nasibulin, A. G.; Kauppinen, E. I.; Brown, D. P.; Jokiniemi, J. K. *J. Phys. Chem. B* **2001**, *105* (45), 11067. (b) Kitchens, C. L.; McLeod, M. C.; Roberts, C. B. *J. Phys. Chem. B* **2003**, *107* (41), 11331. (c) Giuffrida, S.; Condorelli, G. G.; Costanzo L. L.; Fragala, I. L.; Ventimiglia, G.; Vecchio G. *Chem. Mater.* **2004**, *16*, 1260.

(27) Rothe, J.; Hormes, J.; Bönnemann, H.; Brijoux, W.; Siepen, K. *J. Am. Chem. Soc.* **1998**, *120*, 6019.

(28) Drake, I. J.; Fujdala, K. L.; Baxamusa, S.; Bell, A. T.; Tilley, T. D. *J. Phys. Chem. B* **2004**, *108* (48), 18421.

(29) See for example: (a) Chaki, N. K.; Vijayamohanan, K. P. *J. Phys. Chem. B* **2005**, *109*, 2552. (b) Zhang, Q.; Clark, C. G., Jr.; Wang, M.; Remsen, E. E.; Wooley, K. L. *Nano Lett.* **2002**, *2* (10), 1051. (c) Shenhar, R.; Rotello, V. M. *Acc. Chem. Res.* **2003**, *36* (7), 549 (d) Ang, T. P.; Wee, T. S. A.; Chin, W. S. *J. Phys. Chem. B.* **2004**, *108* (30), 11001. (e) Vyazovkin, S. *Anal. Chem.* **2004**, *76* (12), 3299.

(30) Yang, S.; Navrotsky, A. *Chem. Mater.* **2004**, *16* (19), 3682.

(31) Craft, B. C.; Feldman, M.; Morikawa, E.; Poliakoff, E. D.; Saile, V.; Scott, J. D.; Stockbauer, R. L. *Rev. Sci. Instrum.* **1992**, *63*, 1561.

(32) Koningsberger, D. C.; Prins, R. *X-ray Absorption*−*Principles, Applications, Techniques of EXAFS, SEXAFS and XANES*; Wiley and Sons: New York, 1988; Vol. *92*.

(33) Teo, B. K. *EXAFS*: *Basic principles and data analysis*; Springer-Verlag: New York, 1986.

(34) Nilsson, K. B.; Persson, I. *Dalton Trans*. **2004**, 1312.

(35) Kau, L.-S.; Spira-Solomom, D. J.; Penner-Hahn, J. E.; Hodgson, K. O.; Solomon, E. I. *J. Am. Chem. Soc*., **1987**, *109*, 6433.

(36) Cullity, B. D.; Stock, S. R. *Elements of X-Ray Diffraction*, 3rd version; Prentice Hall: Upper Saddle River, NJ, 2001; Appendix 5.